The Influence of Appendages and their Stall on Submarine Hydrodynamic Loads

Gregory J. Seil[1,4] , gregory.seil@dst.defence.gov.au
David Pook[2,4], david.pook@dst.defence.gov.au
Mai Chi Nguyen [1,4] , mai-chi.nguyen@dst.defence.gov.au
Zhi Quan Leong [3,4] , zhi.leong@utas.edu.au

[1] Advanced VTOL Technologies Pty Ltd
[2] School of Engineering, RMIT University
[3]Australian Maritime College, University of Tasmania
[4] Maritime Division, Defence Science and Technology Group

ABSTRACT
Global hydrodynamic loads as a function of drift angle are presented for the Defence Science and Technology Group (DST) generic submarine geometry BB2. Loads are calculated for a model-scale Reynolds number using Computational Fluid Dynamics (CFD) at angles of drift. Abrupt change in the global loads are attributed to appendage stall. Surprisingly, CFD-predicted aft-control-surface (ACS) and bridge fin stall are not easily identified from the sway force. Instead, secondary load components, such as the heave force, must be used to identify that an appendage has stalled. Identifying which ACS has stalled is not possible from global load data. Appendage pressure loads and surface flow topology are required to confirm appendage stall. The results presented will aid the interpretation of experimental load tests currently being conducted by DST.

INTRODUCTION
When a submarine manoeuvres and is at an angle-of-incidence to the oncoming flow, the global forces and moments may exhibit both linear and non-linear variation with incidence angle. For example, at an angle-of-drift (AoD), the sway force, roll moment and yaw moment acting on the submarine exhibit (near) linear variation for small AoD changes. The heave force and pitch moment exhibit a non-linear (quadratic) variation with AoD. Another form of non-linearity is the abrupt load changes that can occur as individual appendages stall.

Appendage stall has implications for the prediction of manoeuvring performance and the design of control systems. It makes the prediction of manoeuvring performance difficult for two reasons: the first is the need for the manoeuvring model to account for abrupt changes in the hydrodynamic forces and moments; the second is reduced confidence in the force and moment prediction due to difficulties predicting stall and post stall loads accurately. Post stall, hydrodynamic loads may vary significantly as a function of time due to unsteadiness in regions of separated flow. Reynolds number effects may also be significant. For stable operation of the boat and the design of its control system, it is therefore essential to be able to predict incidence angles when abrupt changes in global forces and moments occur.

Prediction of appendage stall with semi-empirical methods is often not reliable or possible. Determination of appendage stall from experiment can also be difficult. For example, from the DARPA Suboff load data in Roddy [1], bridge fin stall can be inferred for a drift angle of approximately 16°. This is done by examining loads data for the Suboff tested without the aft control surfaces (ACS), and identifying the abrupt change in the sway force that must be attributed to bridge fin stall. However, due to the effect of the bridge fin wake and trailing vortex when at an AoD, the stall of the ACS cannot be found experimentally by removing the bridge fin. This can make determination of a given appendage stall, or attributing abrupt changes in global loads to the stall of a given appendage, impossible without some other measurement quantity (e.g. surface flow topology).

The data from Mackay [2] for the `Standard Submarine Model' geometry, which tested the same submarine geometry in multiple facilities to assess load dependency on facility and experimental procedures, again identified bridge fin stall by tests without the ACS. However, bridge fin stall varied from approximately 12° AoD to in excess of 20° depending on the test conditions. Stall of the hull and ACS only configuration was reported as possibly visible in only one data set, for an AoD of approximately 20°. This result suggests that appendage stall might be difficult to discern from experiments that measure only global loads.

The Defence Science and Technology Group (DST) generic submarine geometry BB2 is currently undergoing experimental testing to determine loads. A priori knowledge of appendage stall, and how it manifests in global load measurements, will aid the interpretation of experimental results. Computational Fluid Dynamics (CFD) potentially offers the ability to predict appendage stall, and possibly even boat loads post appendage stall. However, experimental validation of CFD-predicted appendage stall, and how it manifests in the measured global loads, will be required.

In this paper, the non-linear changes in the force and moments on the BB2 submarine with AoD are predicted using CFD. Abrupt, non-linear changes in loads predicted by CFD are related to the stall of appendages. Stall is determined by examining the pressure loads and surface flow topology on individual appendages. The results presented, when combined with future BB2 experimental data, will be used to validate CFD prediction of submarine appendage stall and increase confidence in submarine hydrodynamics and manoeuvring based on CFD predictions.

DST GROUP EVOLVED GENERIC SUBMARINE GEOMETRY (BB2)

The DST submarine geometry (BB2) is shown in Figure 1. The full-scale BB2 has a submerged displacement of 4343 m^3, an overall length of 70.2 m, and a maximum hull diameter of 9.6 m with a 10.6 m distance from the keel to the top of the casing. The bridge fin has a span of 5.6 m and a chord of 11.0 m.

The BB2 features an X-form arrangement of the ACS and forward hydroplanes mounted on the bridge fin. The X-form ACS arrangement extends to the "bounding box" [3] defined by the width and depth of the hull. The BB2 has been tested to verify that it has straight line stability (Overpelt et al. [4]).

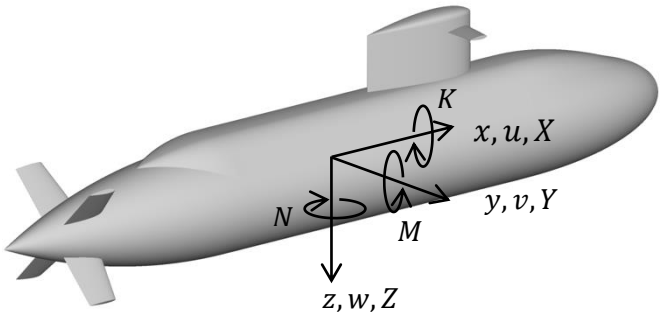

Figure 1 DST Group Evolved Generic Submarine Geometry (BB2) and the body-fixed coordinate system with its origin located amidships.

AXIS SYSTEM

The body-fixed Cartesian coordinate system (x, y, z) used to define the positive direction of the forces (X, Y, Z), moments (K, M, N), and linear velocity (u, v, w) is shown in Figure 1. The origin of this axis system is located amidships. Moments are reported about amidships.

COMPUTATIONAL FLUID DYNAMICS MODELLING

ANSYS Fluent 14.5 was used for the CFD simulations, with closure of the Reynolds Averaged Navier-Stokes (RANS) equations provided by the shear-stress transport (SST) $k-\omega$ turbulence model [5]. Second-order upwind differencing was used for the convective terms in the governing momentum equations, and the turbulence quantities k and ω. Diffusion terms used a second-order central difference. The SIMPLE algorithm was used for pressure-velocity coupling.

The submarine was modelled at a depth absent of free-surface effects using a rectangular domain of length $6.0L$ and lateral dimensions $3.0\ L \times 3.0\ L$. The submarine was placed on the centreline of the domain, $2.0\ L$ from the upstream boundary condition. A fully structured grid of 60.9 million cells was generated for the domain surrounding the submarine using Pointwise V17. Figure 2 shows the surface grid on the submarine, as well as the grid on the centre plane of the flow domain.

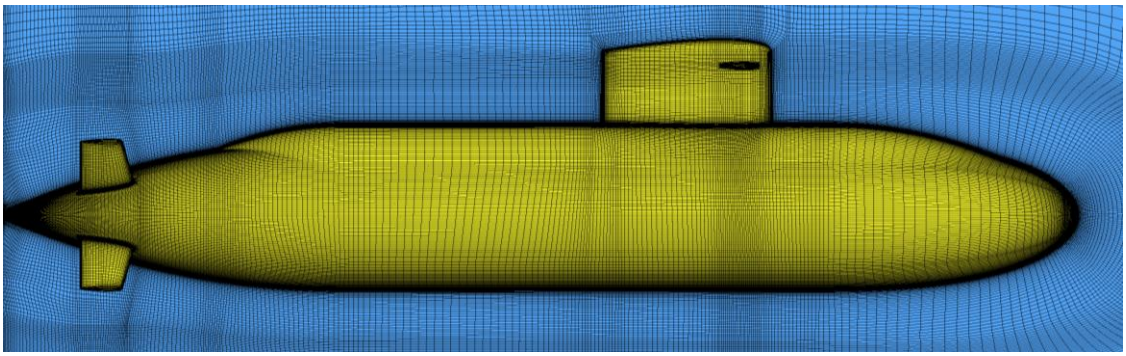

Figure 2 Surface grid of BB2 CFD model and grid on the domain centre plane.

All sides of the rectangular domain were specified as uniform velocity-inlet boundary

conditions. An AoD was created by changing the direction of the flow at the velocity-inlet boundary conditions. A turbulence intensity of 1%, and ratio of turbulent viscosity (μ_t) to dynamic viscosity (μ) of 10 was specified at the velocity-inlet boundary conditions. All surfaces of the submarine were specified as non-slip walls.

The freestream speed, density and dynamic viscosity were set to achieve the desired Reynolds number given by,

$$\mathrm{Re} = \frac{\rho U L}{\mu}, \tag{1}$$

where ρ is the fluid density, U the freestream speed and L the length of the boat. All calculations were performed for a model-scale Reynolds number of 5.2×10^6. For this Reynolds number, the average y^+ with the grid used was less than 1.

CFD modelling was performed for a range of drift angles (β) from 0° to 20°. The drift angle is defined as,

$$\beta = \tan^{-1}\left(\frac{-v}{u}\right). \tag{2}$$

A positive drift angle implies the flow is from the port side.

Grid Sensitivity

A comprehensive grid sensitivity was undertaken for the current grid by Seil et al. [6], for drift angles of 0°, 10° and 15°. Five grids with total cell counts of 12.9, 29.9, 60.9 (baseline), 122.5 and 250.2 million cells were used in the refinement study. Each successively finer grid had approximately double the number of cells. The methodology of Eça and Hoekstra [7] was used to assess the numerical uncertainty associated with the baseline grid. It was found that for 10° AoD, the forces calculated on the 60.9 million cell grid were within 2% of the Richardson extrapolated grid independent values, and moments within 1.2%. At this AoD, the surface flow on the boat is predominantly attached. For 15° AoD, it was difficult to assess the numerical uncertainty because the forces and moments did not exhibit asymptotic convergence. However, the dominant sway force and yaw moment on the 60.9 million cell grid were within 1.1% of the values obtained on the finest grid. The greatest difference was for the pitch moment, which was within 8.1% of the value on the finest grid. It was thus concluded that for AoD ≤10°, the 60.9 million cell baseline grid produces a solution which is relatively insensitive to further grid refinement. This grid was considered suitable for the study presented in this paper.

RESULTS

The variation of the global forces and moments acting on the boat at an AoD are shown in Figure 3. The forces and moments have been non-dimensionalised according to,

$$X' = \frac{X}{\frac{1}{2}\rho U^2 L^2}, \quad Y' = \frac{Y}{\frac{1}{2}\rho U^2 L^2}, \quad Z' = \frac{Z}{\frac{1}{2}\rho U^2 L^2}, \tag{3}$$

$$K' = \frac{K}{\frac{1}{2}\rho U^2 L^3}, \quad M' = \frac{M}{\frac{1}{2}\rho U^2 L^3}, \quad N' = \frac{N}{\frac{1}{2}\rho U^2 L^3}, \tag{4}$$

where X, Y, Z is the surge, sway and heave forces, and K, M, N is the roll, pitch and yaw moments. The variation of the non-dimensional pressure force magnitude (F'_P) acting on

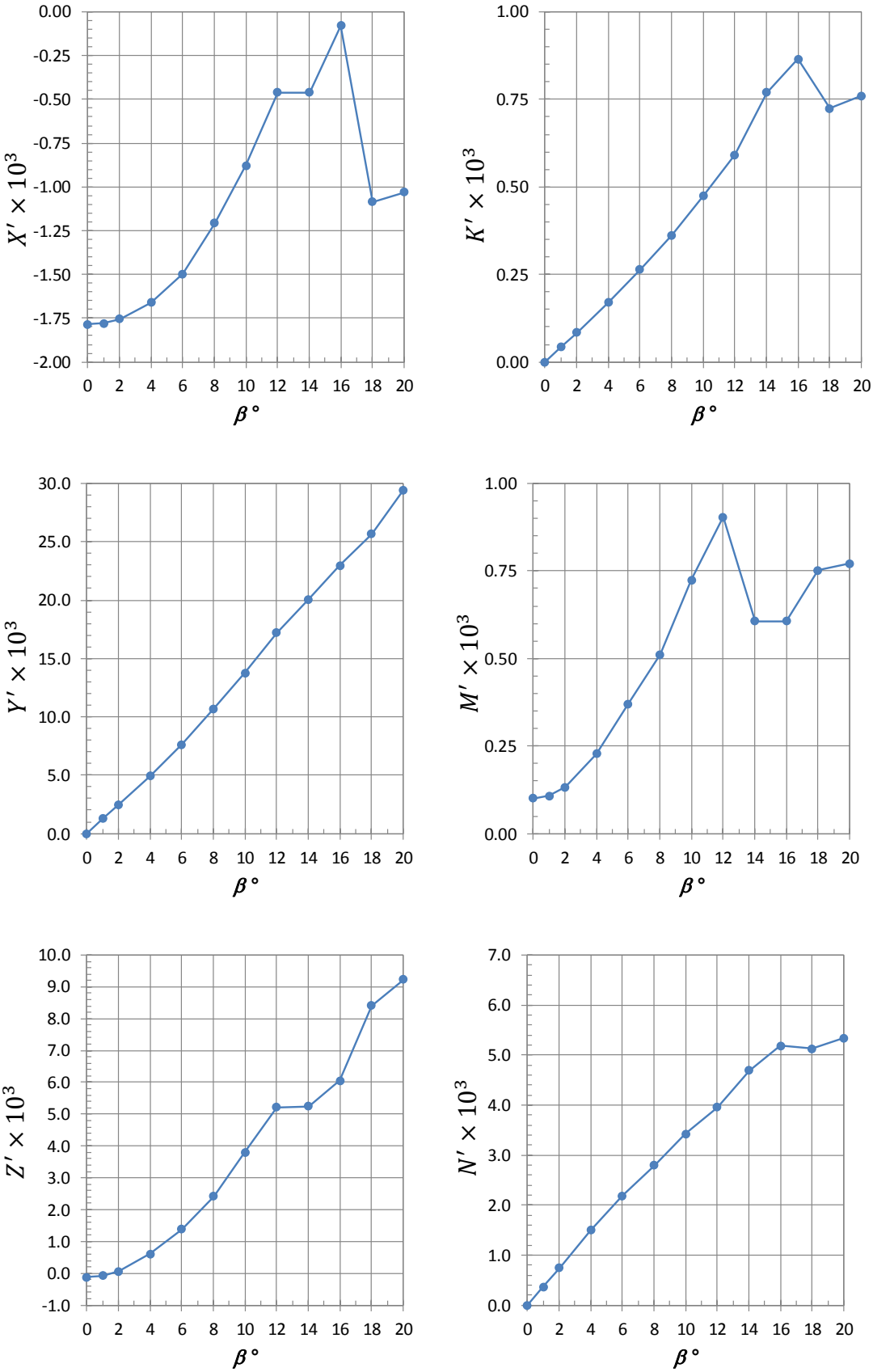

Figure 3 Variation of global forces and moments acting on the BB2 with AoD.

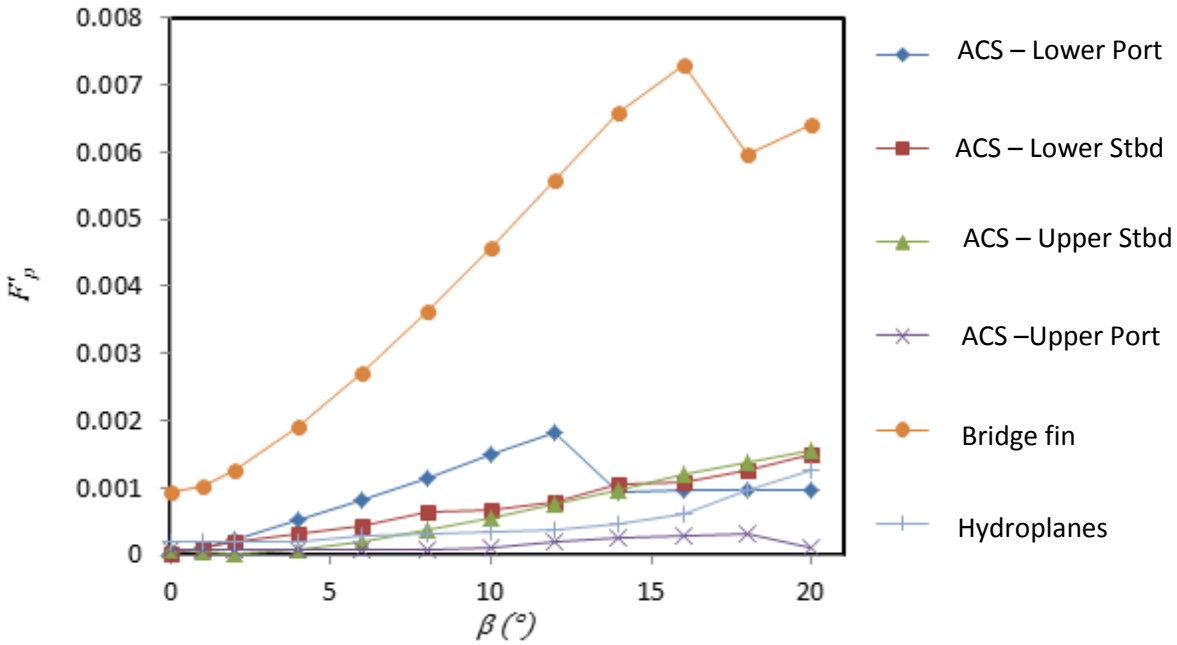

Figure 4 Variation of pressure force magnitude on the BB2 appendages with AoD. Port is the windward side.

each appendage is shown in Figure 4. This pressure force is obtained by integrating the static pressure over the wetted area of the appendage and then non-dimensionalising this force by $(\frac{1}{2}\rho U^2 L^2)$, consistent with (3).

Abrupt, non-linear changes in the global forces and moments seen in Figure 3 can be related to stall on the appendages by examining the changes in the pressure force shown in Figure 4. Further support for appendage stall is found by examining the skin friction topology on the hull and its appendages, shown in Figure 5 to Figure 7. The skin friction lines can indicate regions of separated flow.

From Figure 3, for an AoD less than 12°, the heave force and pitch moment produce a stern-dipping tendency. The first abrupt load change occurs between an AoD of 12° and 14° and is clearly visible in the surge, heave and pitch (which are not the dominant loads, i.e. sway and yaw). The pressure force magnitude variation on each appendage in Figure 4 suggests that the lower port (windward) ACS stalls with the first abrupt load change between 12° and 14°. Stall is indicated by the reduction of the pressure force at a larger AoD.

Figure 5 confirms the stall with the dramatic change in the surface flow topology on the leeward side of this ACS. For 12° AoD, the flow is attached over most of the ACS chord, except near the trailing edge. For 14° AoD, a large region of reversed flow is clearly seen extending from the ACS root and trailing edge, covering a significant portion of the ACS span. Reversed flow is indicated by skin friction lines with a component directed upstream. Interestingly, the global sway force in Figure 3 does not show an abrupt change with this ACS stall. This is attributed to the large sway load created by the hull-casing relative to the small sway force of a single ACS. However, the abrupt change is visible in the global heave

force as the ACS produces a relatively significant heave force compared to the hull when the boat is at an AoD.

The pressure magnitude curves in Figure 4 show the next appendage to stall is the bridge fin, between 16° and 18° AoD. Figure 6 shows the dramatic change in flow topology on the leeward side of the bridge fin between these drift angles. For 16° AoD, a complex flow surface flow topology exists, due in part to the interaction with the bridge fin hydroplane which results in flow separation on the underside of the hydroplane and the formation of two vortices at the indicated foci. The flow around the leading edge of the bridge fin remains attached. For 18° AoD, the flow separates immediately downstream of the bridge fin leading edge and a large region of reversed flow covers most of the leeward side. The reversed flow region also extends onto the adjacent casing.

From Figure 3, the bridge fin stall is accompanied by abrupt changes in all global load components except the sway force. Again, this attributed to the sway force of the hull being significantly greater than that of the bridge fin.

The pressure force magnitude curve for the lower starboard (leeward) ACS in Figure 4 is quite non-linear but no clear indication of stall is seen. Plateaus in the pressure force are seen between 8° and 10° AoD, and 14° and 16° AoD. Surface flow topology for this ACS is shown in Figure 7. Between 8° and 10° AoD, a corner separation develops.

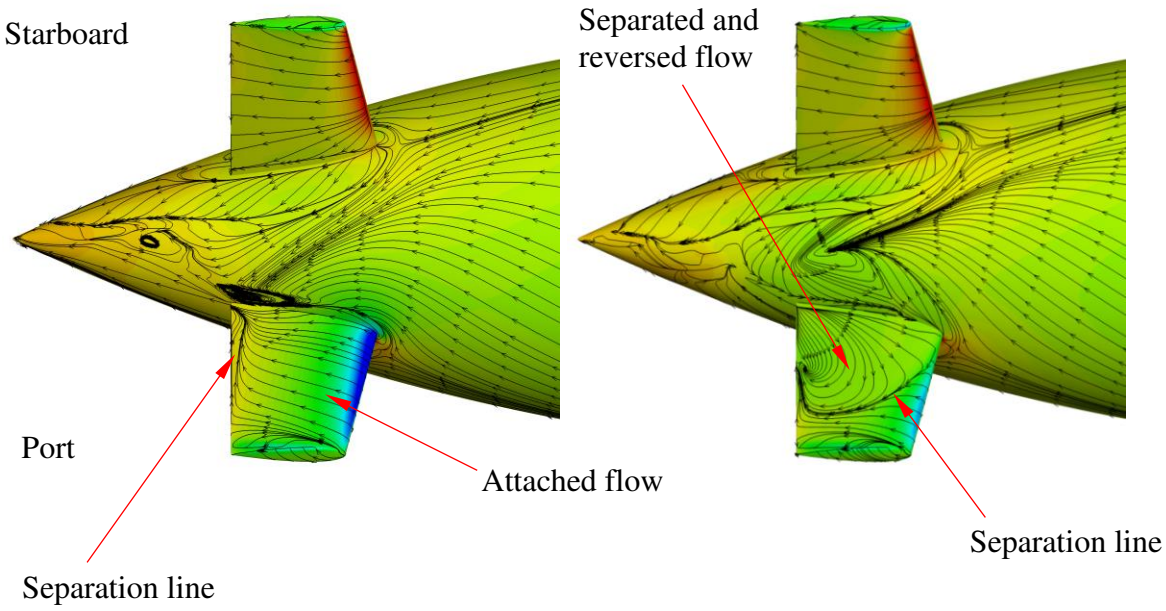

a) β=12° b) β=14°

Figure 5 Surface skin friction lines showing flow topology in the vicinity of the lower port (windward) ACS, view from the underside of the hull. Contours are static pressure (red high, blue low, values not shown)

Between 10° and 16° AoD, the corner flow separation grows in size, and by 16° AoD it reaches the full span of the ACS, but only along the trailing edge. However, the larger pressure force magnitude with greater AoD indicates the ACS is not stalled.

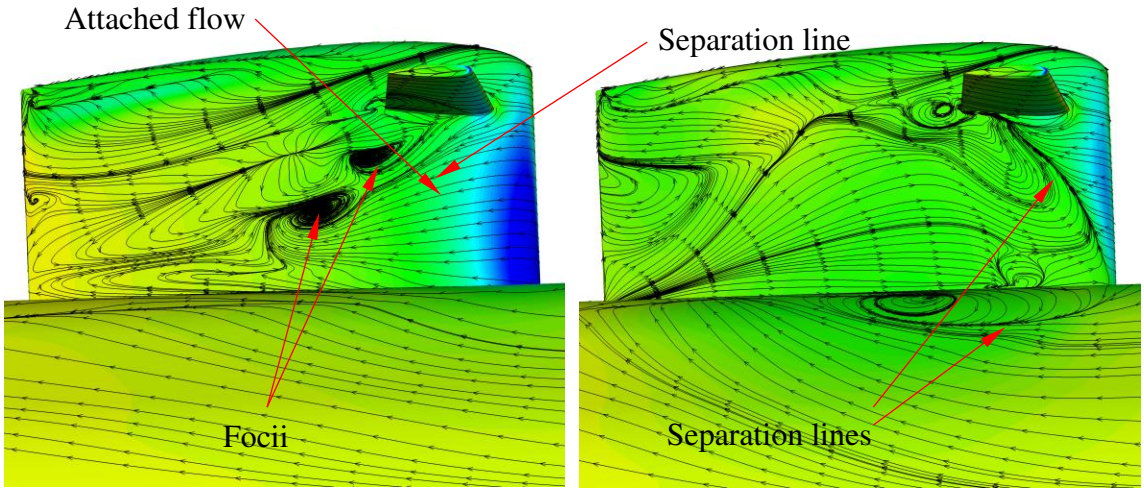

a) β=16° b) β=18°

Figure 6 Surface skin friction lines showing surface flow topology on the leeward side of the bridge fin. Contours are static pressure (red high, blue low, values not shown).

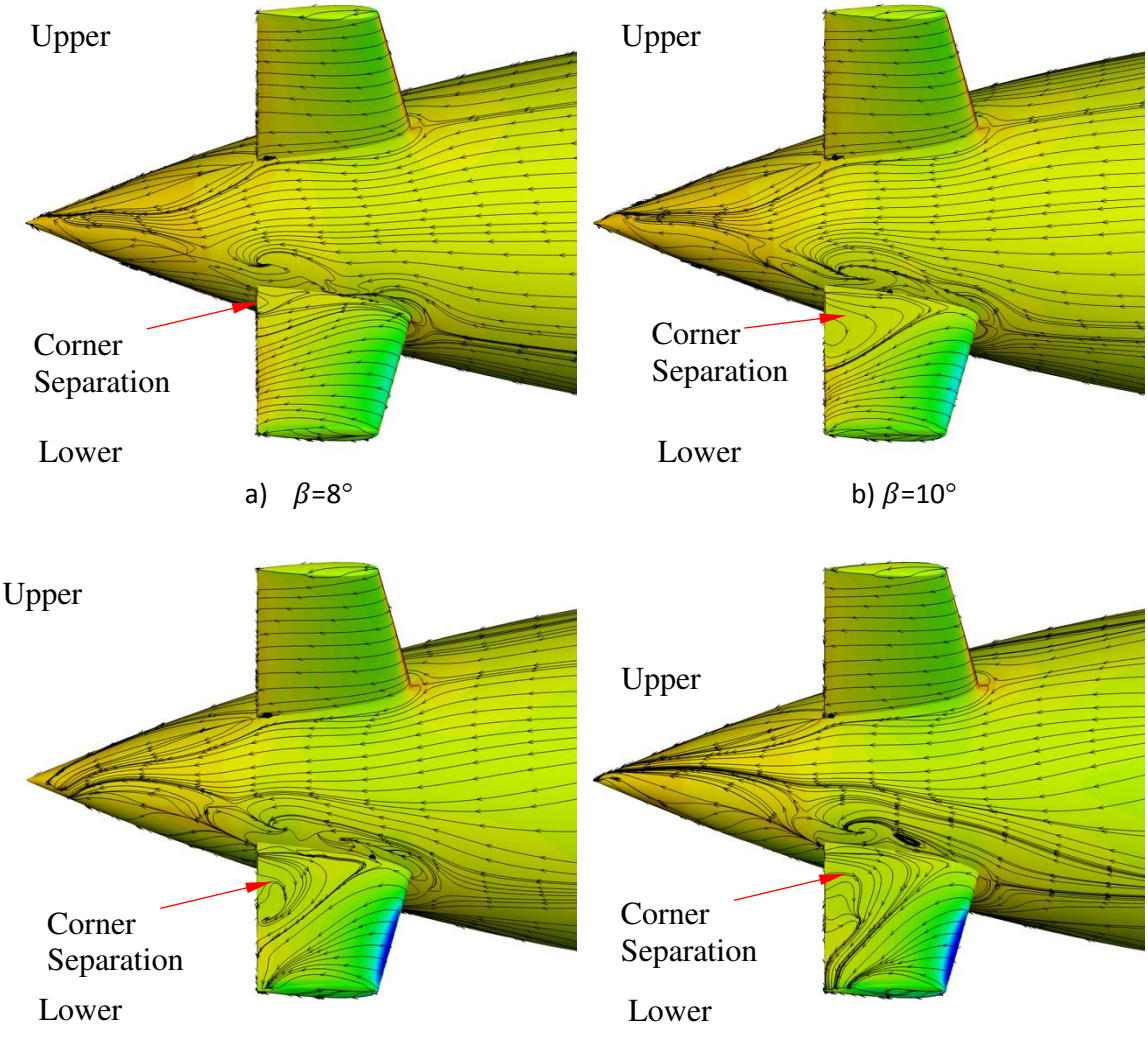

a) β=8° b) β=10°

c) β=14° d) β=16°

Figure 7 Surface skin friction lines showing flow topology in the vicinity of the lower starboard (leeward) ACS, view from starboard. Contours are static pressure (red high, blue low, values not shown).

The pressure force magnitude of the upper port ACS is seen in Figure 4 to reduce significantly between 18° and 20° AoD. However, surface flow topology (not shown) again does not indicate a stall

DISCUSSION

The results presented demonstrate the abrupt changes in global loads are due to appendage stall. The CFD predicted order of appendage stall in the AoD range studied is:

1) Lower port (windward) ACS: $12° \leq \beta < 14°$,
2) Bridge fin: $16° \leq \beta < 18°$.

The lower port ACS stalls at the lowest AoD due to the crossflow over the hull and the tip vortex of the bridge fin interacting with the ACS. The blockage effect of the hull accelerates the crossflow on the windward side. This increases the incidence seen by both port (windward) ACS If the bridge fin and casing were absent, then the incidence increase on the upper port ACS would be identical. However, trailing flow structures from the bridge fin (e.g. tip vortex) induce circulation around the hull and alter the incidence seen by the upper and lower port ACS. The bridge fin wake structures create an anticlockwise, when viewed from stern, circulation around the hull which decreases the incidence on the upper port ACS and increases the incidence of the lower port ACS. Hence, the stall of the lower port ACS is at a lower AoD than the bridge fin.

Stall of the bridge fin will be influenced not only by its design (e.g. hydrofoil cross-section) but also by the increased incidence due to the hull blockage effect. Again, hull-blockage accelerates the crossflow past the bridge fin, effectively increasing the incidence. The stall of the bridge fin at a higher AoD than the lower port (windward) ACS can be attributed to its lower aspect ratio (approximately 0.5 based on exposed area) compared to the aspect ratio of a single ACS (closer to 2), as well as the bridge fin's wake increasing the lower port (windward) ACS incidence.

It is interesting that, despite the use of ACS to generate sway and yaw for stability or control, stall of the lower port ACS is not readily visible in the global sway and yaw curves. The abrupt change in the global heave force is the clear indicator of stall. However, which ACS had stalled is not identifiable from global loads. In an experiment, supplementary measurements would be required, e.g. individual appendage loads or surface flow topology. Even more surprising is that the stall of the bridge fin is not clearly visible in the global sway force. Reliable identification of stall from experimental loads will likely require CFD to confirm individual appendage stall, assuming validation of CFD stall predictions can be obtained.

The pressure force magnitude change with AoD for each ACS varies significantly and is attributable to hull and bridge fin vortex influences as previously discussed. However, the force changes for each ACS, particularly the lower starboard ACS, do not vary `smoothly' with AoD. This appears to be attributable, at least in part, to the changing corner flow separation predicted by the CFD. If the CFD is accurate, then semi-empirical determination of ACS loads and stall is not likely to be accurate. However, the corner flow separation—a wing-body junction flow—cannot be predicted accurately by eddy-viscosity RANS models

(e.g. SST $k-\omega$) [8]. The loads predicted when significant separated flow is present in this CFD study, must be interpreted with caution. However, since the hull and casing are the dominant sources of loads, then large errors in ACS load prediction may not significantly affect global loads. The grid refinement study conducted by [6] for the grid used in this paper, and the minimal separated flow for AoD less than approximately 12°, does provide some confidence in predicted loads at least up to 12° AoD.

CONCLUSION

The CFD modelling in this paper provides an understanding of the flow around the BB2 submarine. The results are relevant to manoeuvring and control system design. The results presented will allow more targeted testing in load experiments currently being conducted on the BB2 geometry at DST.

Over a range of drift angles ($0° \leq \beta \leq 20°$), CFD predicts the BB2 will create highly non-linear global forces and moments. Abrupt load changes are related to appendage stall. Surprisingly, appendage stall was not easily discernible in the dominant sway force. Secondary loads such as the heave force in the case of the ACS, provided a clearer indication of stall. However, identifying which appendage had stalled required the examination of individual ACS loads and surface topology. In an experimental program, global loads would not be sufficient to reliably detect and identify which ACS has stalled.

REFERENCES

1. Roddy, R.F. (1990), "Investigation of the Stability and Control Characteristics of Several Configurations of the DARPA SUBOFF Model (DTRC Model 5470) from Captive-Model Experiments", *David Taylor Research Center*, DTRC/SHD-1298-08
2. Mackay, M. (2003), "The Standard Submarine Model: A Survey of Static Hydrodynamic Experiments and Semiempirical Predictions", *DRDC Atlantic*, TR-2003-079
3. Renilson, M.R. (2015), "Submarine Hydrodynamics", *Springer Briefs in Applied Sciences and Technology*.
4. Overpelt, B., Nienhuis, B. and Anderson, B. (2015), "Free Running Manoeuvring Model Test on a Modern SSK Class Submarine (BB2)", *Proc. Pacific 2016 International Maritime Conference*, Sydney, 6-8 Oct. 2015.
5. *ANSYS Fluent User's Guide*, ANSYS Inc.
6. Seil, G. J., Nguyen, M.C., Pook, D. and Leong, Z. Q. (2017), "CFD Study of the Evolved DST Group Generic submarine (BB2)", *DST Group Technical Report*, Under Review.
7. Eça, L. and Hoekstra, M. (2009), "Evaluation of Numerical Error Estimation based on Grid Refinement Studies with the Method of Manufactured Solutions", *Computers & Fluids*, Vol. 38, pp. 1580-1591.
8. Gand, F., Brunet, V. and Deck, S. (2010), "A Combined Experimental, RANS and LES Investigation of a Wing Body Junction Flow", *40th Fluid Dynamics Conference and Exhibit*, Chicago, 28 Jun-1 Jul.